

Article

The Process of Digital Data Flow in RE/CAD/RP/CAI Systems Concerning Planning Surgical Procedures in the Craniofacial Area

Paweł Turek ^{1,*} , Ewelina Dudek ², Mateusz Grzywa ² and Kacper Więcek ²

¹ Faculty of Mechanical Engineering and Aeronautics, Rzeszów University of Technology, 35-959 Rzeszów, Poland

² Faculty of Mathematics and Applied Physics, Rzeszów University of Technology, 35-959 Rzeszów, Poland; 164230@stud.prz.edu.pl (E.D.); 166774@stud.prz.edu.pl (M.G.); 168488@stud.prz.edu.pl (K.W.)

* Correspondence: pturek@prz.edu.pl

Abstract: This paper presents the process of digital data flow in RE/CAD/RP/CAI systems to develop models for planning surgical procedures in the craniofacial area. At the first RE modeling stage, digital data processing, segmentation, and the reconstruction of the geometry of the anatomical structures were performed. During the CAD modeling stage, three different concepts were utilized. The first concept was used to create a tool that could mold the geometry of the cranial vault. The second concept was created to prepare a prototype implant that would complement the anterior part of the mandibular geometry. And finally, the third concept was used to design a customized prototype surgical plate that would match the mandibular geometry accurately. Physical models were made using a rapid prototyping technique. A Bambu Lab X1 3D printer was used for this purpose. The process of geometric accuracy evaluation was carried out on manufactured prototypes of surgical plates made of ABS+, CPE, PLA+, and PETG material. In the geometric accuracy evaluation process, the smallest deviation values were obtained for the ABS plus material, within a tolerance of ± 0.1 mm, and the largest were obtained for CPE (± 0.2 mm) and PLA plus (± 0.18 mm). In terms of the surface roughness evaluation, the highest value of the Sa parameter was obtained for the PLA plus material, which was $4.15 \mu\text{m}$, and the lowest was obtained for the CPE material, equal to $3.62 \mu\text{m}$. The knowledge of the flow of digital data and the identification of factors determining the accuracy of mapping the geometry of anatomical structures allowed for the development of a procedure that improves the modeling and manufacturing of anatomical structures within the craniofacial region.

Keywords: digital data; reverse engineering; anatomical model; surface roughness; geometry accuracy



Citation: Turek, P.; Dudek, E.; Grzywa, M.; Więcek, K. The Process of Digital Data Flow in RE/CAD/RP/CAI Systems Concerning Planning Surgical Procedures in the Craniofacial Area. *Knowledge* **2024**, *4*, 265–279. <https://doi.org/10.3390/knowledge4020014>

Academic Editor: Jose María Merigo

Received: 18 February 2024

Revised: 17 March 2024

Accepted: 30 April 2024

Published: 15 May 2024



Copyright: © 2024 by the authors. Licensee MDPI, Basel, Switzerland. This article is an open access article distributed under the terms and conditions of the Creative Commons Attribution (CC BY) license (<https://creativecommons.org/licenses/by/4.0/>).

1. Introduction

Currently, the traditional way to design machine parts is to use computer-aided design (CAD) systems [1]. A problem in the design and manufacturing process arises when we have a physical part but do not have technical documentation for it (e.g., digital data describing the model's geometry). The only way to solve this problem is through the reverse engineering (RE) process [2–4]. This process consists of digitizing the data, reconstructing the geometry, CAD modeling, and possibly manufacturing the physical model again, using, among other things, rapid prototyping (RP) techniques. Currently, the reverse engineering process is used in many fields, including aerospace [5], automobiles [6], and architecture [7]. One of the directions of RE development is also a combination of medical imaging techniques and typical engineering modeling. This approach has resulted in 3D models of anatomical structures [8], surgical templates [9], and implants [10], which are used in many medical fields, including cardiology [11], orthopedics [12], facial surgery [13,14], and dentistry [15].

Modeling bony structures is increasingly becoming the foundation for planning complex procedures in the craniofacial area [13,16]. Based on medical knowledge, it is possible to specify the facial regions of the skull that are subject to the most frequent damage [13]. These include the nasal bone, cranial vault, mandible, orbit, and zygomatic bone [13,17]. Various factors can cause the occurrence of these injuries. The most common include accidents, genetic defects, or cancer. In this case, the efficient transfer of digital data is necessary to finally obtain a tool, such as a surgical template, that allows for the accurate performance of surgery within the facial area [8,9]. In modeling anatomical structures of the craniofacial region, the first step is related to acquiring volumetric data using, e.g., tomographic medical systems [9,14]. The collected data are then converted to a digital 3D model in RE systems and further edited in CAD systems. The physical model can be obtained using computerized manufacturing techniques.

A key aspect of modeling anatomical structures is to ensure the adequate numerical accuracy of the structure, as errors in the digital model are reproduced later in the manufacturing process, which, in the case of implants, finally determines how well the defect matches the patient's actual anatomical structure [18,19]. The most significant influence on the accuracy of the model is the acquisition stage of the tomographic data [20,21]. The critical parameters in this case are the spatial and contrast resolution of the Digital Imaging and Communications in Medicine (DICOM) data. Further enhancement of DICOM data quality is achieved through digital filtering involving contrast enhancement, edge sharpening, and noise removal [22]. Often, a data interpolation process is also performed, which improves the spatial resolution of DICOM data [14,23]. For the RE modeling process, an essential factor affecting accuracy is the process of segmentation and geometry reconstruction [24,25]. CAD systems also play a crucial role in medical modeling processes, in which, on the one hand, surgical instruments and implants are designed, and, on the other, digital data are finalized for manufacturing [26,27]. This purpose must remove programming errors in the digital files. In the case of a model saved to the Standard Triangulation Language (STL) format, the most common errors include the incorrect orientation of triangles, duplicate edges and vertices, and duplicate triangles [22,25]. For a model saved to the STandard for the Exchange of Product model data (STEP) format, it is crucial to achieve geometric continuity between adjacent parameterized surface patches [28–30]. Correctly generating a digital model in the STL or STEP format allows for the production of the final model. Due to the geometric complexity of models of anatomical structures, RP methods are often used. These methods involve creating a model by applying successive layers of material. Computer-aided inspection (CAI) is usually performed to verify the manufacturing process. For this purpose, manual tools [31], contact [32,33], and optical coordinate measuring systems [8,14,34] are used. Digital data obtained through measurement often allow for dimensional and geometric inspection [14,35] and surface roughness [36,37].

Based on the analysis of the state of the issue, it is reasonable to carry out research, on the one hand, to improve the flow of digital data in RE/CAD/RP/CAI systems and, on the other hand, to identify the factors determining the accuracy of the geometry of the anatomical structure, surgical template, and implant. It is particularly important to carry out studies in the craniofacial region, which includes bone tissues with very complex geometries. Adequate knowledge and skills in medicine and technical sciences are needed to allow for the full use of currently available tools in the processes involved in reconstructing the facial areas of the skull. Knowledge of the flow of digital data and identifying factors that determine the accuracy of the geometry of anatomical structures can allow for the development of a procedure that will significantly accelerate and improve the modeling and manufacture of anatomical structures within the craniofacial region.

2. Materials and Methods

The 2D images acquired using tomographic diagnostic systems commonly visualize the craniofacial area [9,14]. In this case, the research was conducted on three patients scanned on a Somatom Definition AS+ multi-row CT scanner (Siemens Medical Solutions,

Forchheim, Germany). In the first patient's case, one needed cranial vault restoration while two required mandibular model implants. The tomographic system creates a cross-sectional image of the object by mathematically reconstructing the measured radiation intensities received by detectors moving in a circular orbit around the patient. Some emitted photons passing through the object under study are transmitted, and some are absorbed or scattered. Each tissue has a different X-ray attenuation coefficient. These are normalized to the coefficient for water and expressed in Hounsfield units (HUs). The CT image represents HUs and is presented in grayscale for each pixel. The final output is DICOM data. This is a standard that defines the format and method of image data transmission between imaging devices and units for their analysis and secondary processing (diagnostic descriptive workstations) or archiving systems. An object in DICOM format is multi-attribute. It consists of elements such as first name, last name, and patient ID, as well as a unique attribute that contains image data. During the measurement process, the traditional scanning protocol followed for the craniofacial area was used for the three patients analyzed (Table 1).

Table 1. Scanning protocols.

Parameters	Patient 1	Patient 2	Patient 3
Tube voltage	120 kV	100 kV	80 kV
Tube current–time product	158 mAs	158 mAs	227 mAs
Slice collimation	32 × 1.2 mm	32 × 1.2 mm	64 × 0.6 mm
Kernel	H31s	H31s	I26s
Matrix size		512 × 512	
Pixel size		0.4 mm × 0.4 mm	
Slice thickness	1.5 mm	1.5 mm	0.7 mm

2.1. RE Modeling Process

Due to the limitations of the obtained DICOM data (Figure 1a) [20,21], the spatial and contrast resolution of 2D images was increased before the segmentation process. First, a data interpolation process was carried out. This process consisted of determining additional pixels along with their value based on the intensity of neighboring pixels. This procedure made it possible to obtain a more accurate representation of the contours of the reconstructed bone structure. The data were then subjected to a process of de-noising and edge sharpening. A segmentation was carried out on this reformatted DICOM data (Figure 1b).



Figure 1. DICOM data of the craniofacial area: (a) without processing; (b) with numerical processing performed.

The process involved dividing the 2D image into different regions (masks), with each defining a particular anatomical structure [24,25]. This process is usually carried out using manual or semi-automatic methods. In the case of the presented research, a thresholding method was used to segment the bone structures. It consisted of converting a grayscale image into a binary image by setting a binarization threshold. A lower segmentation threshold was selected for the reconstructed geometries: 300 HU for all analyzed patients. The isosurface, a surface rendering method, was used to create the 3D model of the mandible [14,23]. This is based on the marching cube algorithm. This algorithm processes pixel intensity information and uses it to create triangular meshes that map the surfaces of objects reconstructed from DICOM data. The result was 3D visualizations of the models, which were saved in STEP format (Figure 2).

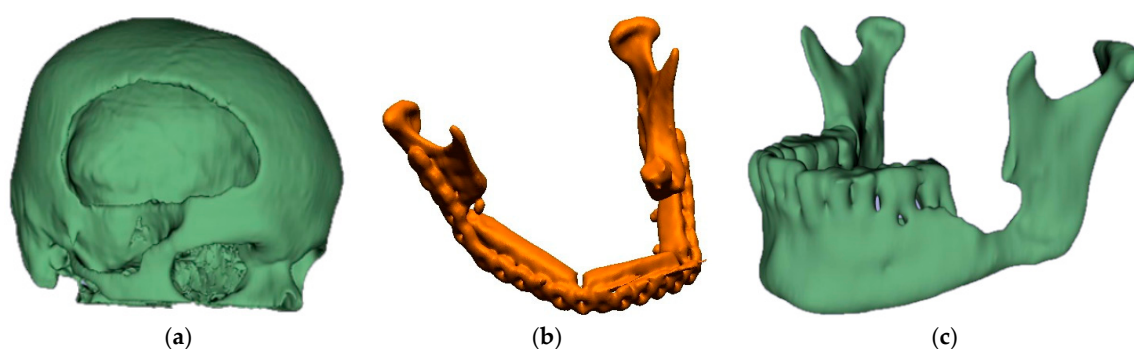


Figure 2. Three-dimensional visualization of DICOM data for (a) Patient 1, (b) Patient 2, and (c) Patient 3.

When creating an STL file [25], a three-dimensional object is described using triangulated surfaces. The STL file describes the surface by specifying the normal vector and the coordinates of the triangle's three vertices. The triangles generated often vary in size and shape. When the conversion process is correct, the defined normal vector should always be directed to the outside of the approximated solid. In converting DICOM data to a 3D STL model, thousands or even millions of triangles are often generated with varying degrees, allowing for the accurate approximation of curvilinear surfaces.

2.2. CAD Modeling Process

In the CAD modeling stage, three concepts were used to create the model: a tool to mold the geometry of the cranial vault, a prototype implant to complement the anterior part of the mandibular geometry, and a customized prototype surgical plate to match the mandibular geometry.

The preliminary CAD modeling of the tool to form the geometry of the cranial vault defect was carried out in Meshmixer. The process at this stage consisted of mirroring against the sagittal plane. A cavity completion model was initially developed and exported using Boolean methods to STL format. Further CAD modeling of the cavity was carried out in CATIA V6. A surface model was created using the automatic surface generation function. Then, a final 3D CAD model was developed by applying functions for solid modeling. In the next step, a mold model was created. It was made by applying Boolean methods to the developed 3D CAD model of the cranial vault defect [38,39]. In addition, a handle and hinges for the mold were created in the modeling process. Finally, all developed models were saved in STEP format. The entire CAD modeling process is presented in Figure 3.

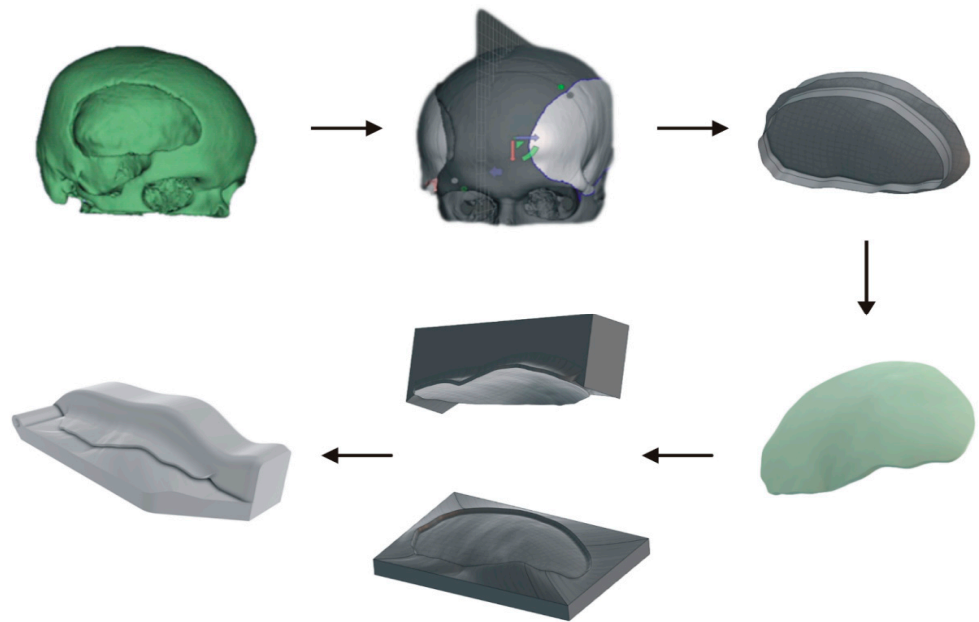


Figure 3. CAD modeling process of a mold for creating a cranial vault defect.

In developing a prototype implant of the anterior part of the mandible (Figure 4), it was necessary to reconstruct the geometry of two mandible models of the same patient (before and after resection) [14]. The two models were then imported into Meshmixer software and fitted. This step determined resection sites using the digital model of the mandible from before the surgery. Basic Boolean functions were used for this purpose. Once the process of modeling the initial geometry of the prototype implant was completed, the process of verifying the model’s fit to the digital geometry of the mandible after the resection procedure began.



Figure 4. CAD modeling process of the prototype implant of the anterior part of the mandible.

Because the human body is not symmetrical, additional tools were necessary for positioning the prototype [14]. These were used to move and rotate the implant prototype precisely in space. In the final stage of the modeling process, the focus was on the aspect of

preparing handles and holes for surgical screws. After the entire geometry of the implant prototype was developed, it was saved in STL format.

A prototype model of the surgical plate was designed using CATIA V5 software. The process was carried out based on the reconstructed geometry of the mandible. The mandible model was converted to a 3D CAD model in the first step [26,28]. The next step was to digitally fill the mandibular bone defect to improve the fit of the modeled surgical plate in this area. The surgical plate model was developed using basic free surface sketching tools. A surface model was then developed based on the functions used for CAD modeling, which was then converted into a solid model. In the final step, the holes for the surgical screws were modeled. As a result, a prototype implant was developed that matched the geometry of the damaged part of the mandible. The anatomical model of the mandible and the resulting surgical plate model were saved in STEP format. The entire CAD modeling process is presented in Figure 5.

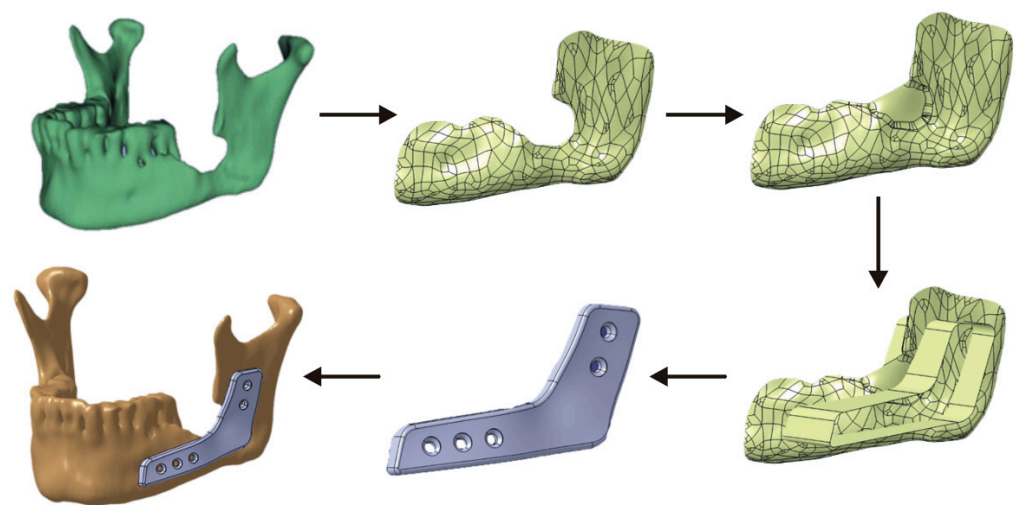


Figure 5. CAD modeling process of a prototype of a customized surgical plate.

2.3. The Process of Manufacturing Models Using Rapid Prototyping (RP) Methods

In the next step, physical models were made using a rapid prototyping technique. For this purpose, a Bambu Lab X1 printer was used. Manufacturing a model using this method consisted of applying successive layers of material until the entire model was obtained [1]. The material applied through the printing nozzle was in a plastic state and permanently bonded to the previously applied layer. The models developed at the CAD modeling stage were prepared in STEP format before printing in OrcaSlicer (Figure 6).

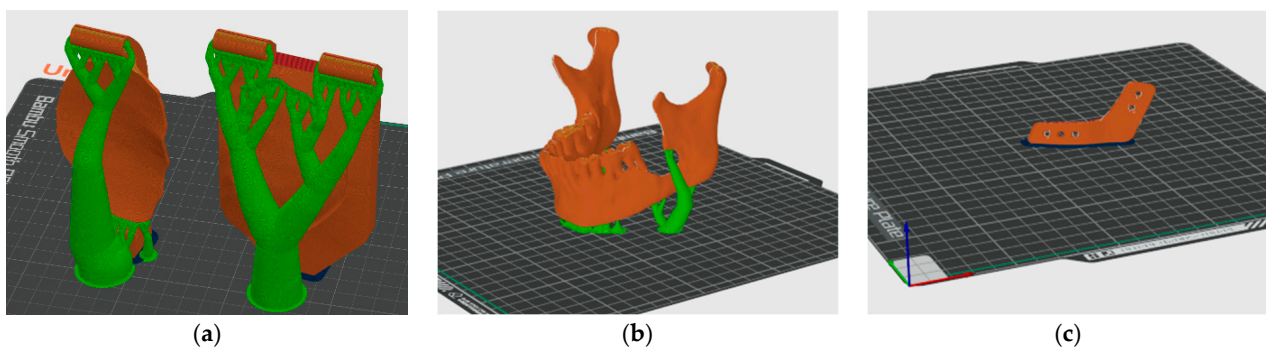


Figure 6. Layering of the model with generated support material for (a) mold elements; (b) mandibular anatomical model; (c) surgical plate model.

The main advantages of the STEP format are the ability to store data using a mathematical representation of curves, good file compression without losing quality with the source files, and backward compatibility. Thus, using a STEP file instead of STL made it possible to achieve the more accurate development of the G-Code controlling the 3D printer. Acrylonitrile butadiene styrene (ABS+), chlorinated polyethylene (CPE), polylactic acid (PLA+), and Polyethylene Terephthalate modified with Glycol (PETG) polymer materials were used in the printing process. The layer thickness was 0.1 mm for the mold component models, and for the mandible and surgical plate models, the value was 0.08 mm. Each material used was calibrated before printing the part. As a result, physical models were obtained (Figure 7).

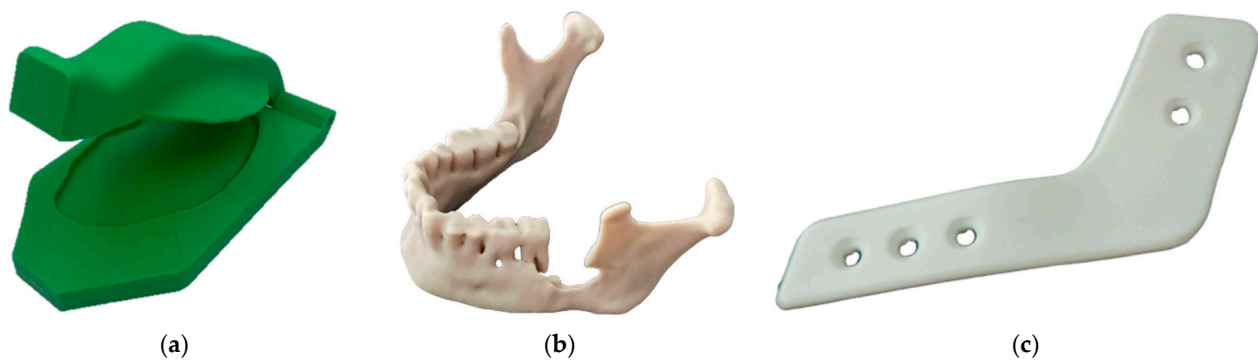


Figure 7. Manufactured models of: (a) mold; (b) mandibular anatomical model; (c) surgical plate model.

2.4. Measurement Process of the Manufactured Models

The process of evaluating geometric accuracy was carried out on manufactured prototypes of surgical plates made of ABS+, CPE, PLA+, and PETG materials. A 7-axis MCA II coordinate measuring arm with a measurement range of 1.8 m, equipped with $MMD \times 100$ laser heads, was used for this purpose [26,27] (Figure 8).



Figure 8. The process of measuring the geometry of a prototype surgical plate.

The measurement plan was determined using Focus Handheld software. The software was also used to communicate and register digital measurement results. A three-dimensional point cloud represented the measurement data. The software also automatically generated a triangle mesh on the collected data based on the obtained data, which was then exported in STL format. The resolution of the point cloud measurement was set to 0.01 mm. To optimize the measurements, the appropriate triangulation distance of the scanner from the measured object was maintained while keeping the laser beam perpendicular to the scanned surface.

The manufactured surgical plate was subjected to surface roughness measurement on a TalyScan 150 measuring machine [27] (Figure 9). In the process of evaluating the surface roughness of surgical templates made of ABS+, CPE, PLA+, and PETG material, a sampling step in the X and Y axes was set equal to 5 μm . The single measured area was 4 mm \times 4 mm. The lowest available measurement speed of 2000 $\mu\text{m/s}$ was used during the measurement. When measuring one profile, the head was not raised before measuring the next. This procedure avoided the introduction of unnecessary tip oscillations during the measurement. The measurement was made perpendicular to the direction of application of successive layers of material. The result was a three-dimensional surface saved to SUR format, on which further numerical processing was carried out.



Figure 9. The process of measuring the surface topography of a manufactured surgical plate.

3. Results

In the case of the presented article, the process of verifying the accuracy of the models' geometry was carried out using Focus Inspection software. The fitting process of the nominal model obtained at the RE/CAD design stage and the reference model generated at the measurement stage using the MCA II measuring arm system equipped with MMD \times 100 laser heads was carried out using the best fit method with an accuracy of 0.005 mm. The evaluation of the geometric accuracy was determined using classical measures of describing the structure of the area. Within the research conducted, the following were determined: mean deviation (y_{average}), standard deviation (σ), maximum deviation (y_{max}), minimum deviation (y_{min}), and range (R). A 3D visualization of the analyzed surface with the obtained parameters is presented in Figure 10.

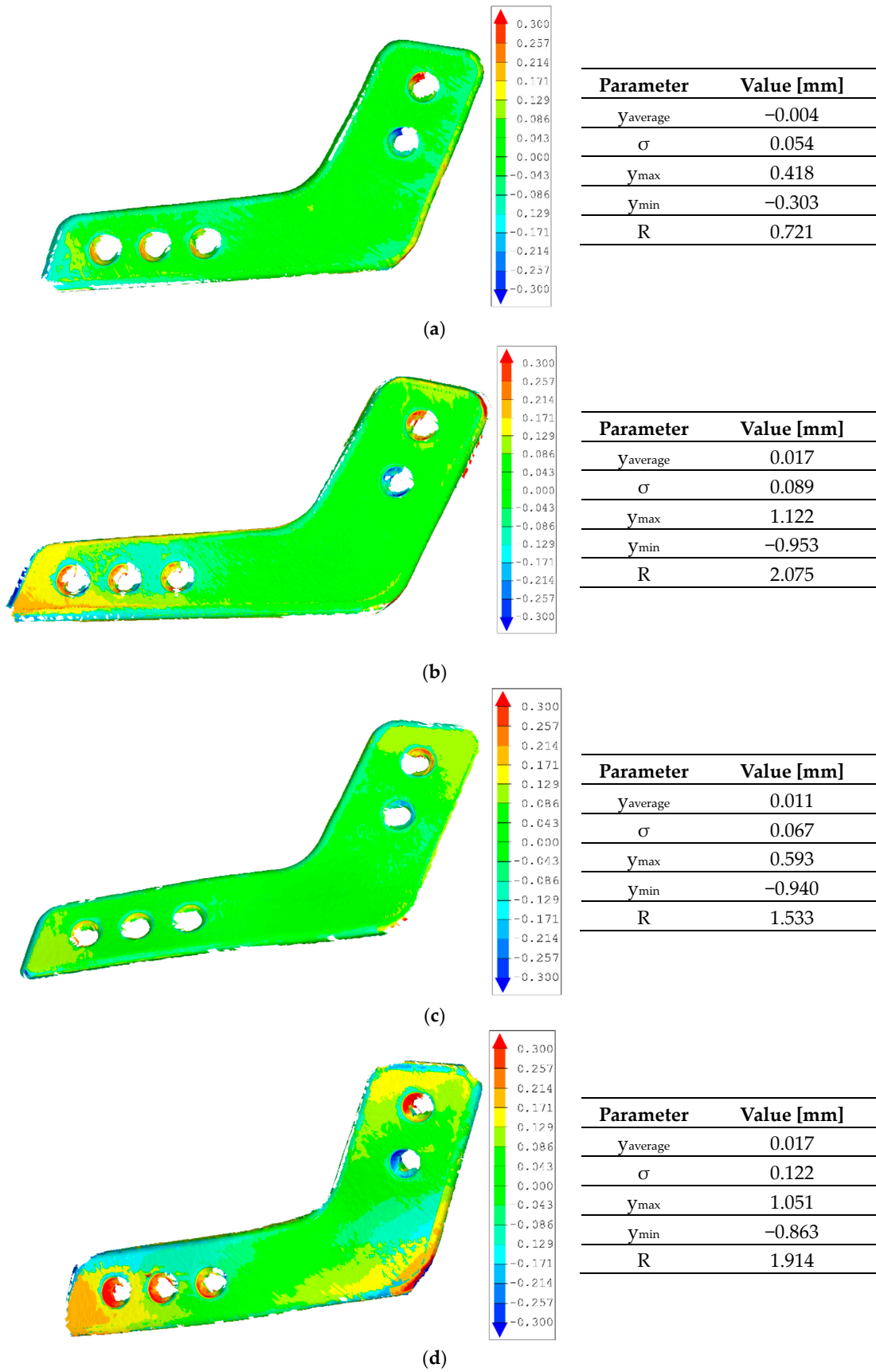


Figure 10. Results obtained evaluating the accuracy of geometry for materials: (a) ABS Plus; (b) PLA plus; (c) PETG; (d) CPE.

After analyzing the geometry measurements of the prototype surgical plate, it was observed that the material used in 3D printing affects the test results obtained. Most of the deviations for the ABS Plus material are within the tolerance of ± 0.1 mm. The deviation map for this material is more uniform, meaning that the deviation values are close to the nominal value. However, an increase in the deviations with a negative value was noticed at the model's edges. Similar results were obtained for the PETG material. The highest geometry deviation values were found for the CPE material and PLA Plus. For the CPE material, most of the deviations are within the tolerance of ± 0.2 mm, and for PLA Plus, the tolerance is ± 0.18 mm. The most significant positive deviations for the PLA Plus and CPE materials were observed in the contact area between the model and the 3D printer's work table, as well as in locations within the surgical screw holes. Despite the system's calibration, problems were encountered with the smooth flow of materials through the print nozzle, making it challenging to produce an accurate representation of the screw holes. The deviations in the contact area between the model and the printer's work table increased due to the difficulty of detaching the prototype wafer after 3D printing. Heterogeneous deviation maps were observed for the PLA Plus and CPE materials. The primary variation in the deviation values was seen in the front part of the surgical plate prototype, which may be related to the faster material shrinkage in this area of the model. All of the reports evaluating the geometric accuracy of the prototype surgical plate are acceptable for the procedure planning process, as they are within the tolerance of ± 0.3 mm.

MountainsMap software was used to determine the surface roughness parameters [27]. First, a filtering process was performed to remove the obtained shape deviations. It was carried out using a third-degree polynomial. Then, to separate the long-wave components, a Gaussian filter $\lambda_c = 0.8$ mm was applied, which marks the transition from roughness to waviness. As a result, a 3D visualization of the surface roughness of the surgical template was obtained. Based on the developed results, the values of the parameters were determined: arithmetic mean height (Sa), squared mean height (Sq), maximum peak height (Sp), maximum valley depth (Sv), and maximum height of the surface (Sz). A three-dimensional visualization of the analyzed surface with the obtained parameters is presented in Figure 11. When analyzing the data evaluating the surface roughness of the studied models, more comparable reports were perceived than in the case of the geometry accuracy analysis. Comparing the obtained 3D visualizations, the layered structure of the analyzed surfaces was noticed. The most significant variability of the measured surface was observed for the PLA plus material. However, the maximum valley depth (Sv) and peak height (Sp) values were obtained for the PETG material, which were also noticeable on the 3D map. The highest value of the Sa parameter was obtained for the PLA plus material, which was $4.15 \mu\text{m}$, and the smallest was obtained for the CPE material, equal to $3.62 \mu\text{m}$. The most negligible variation was the surface obtained from the ABS Plus and CPE materials. For these surfaces, the Sq parameters were $4.56 \mu\text{m}$ and $4.46 \mu\text{m}$, respectively.

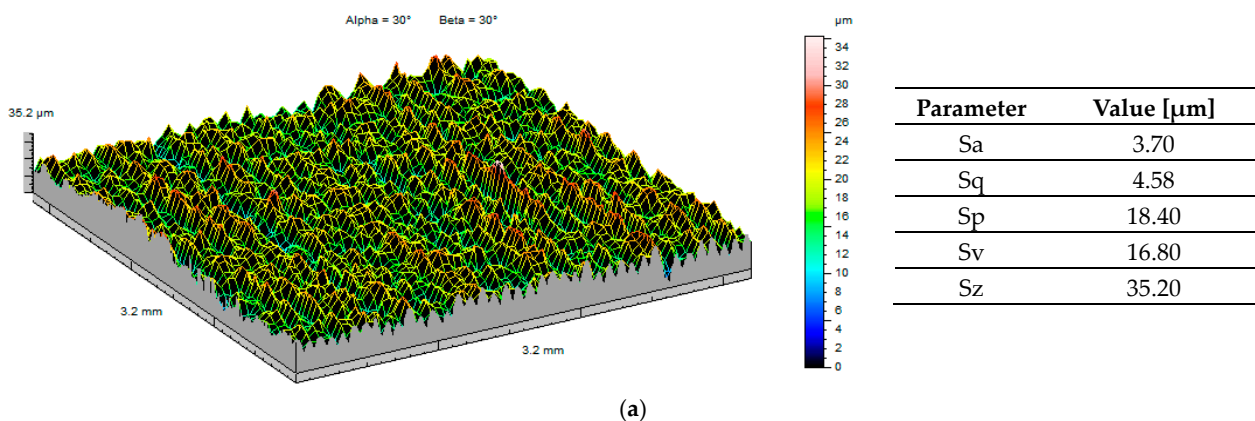


Figure 11. Cont.

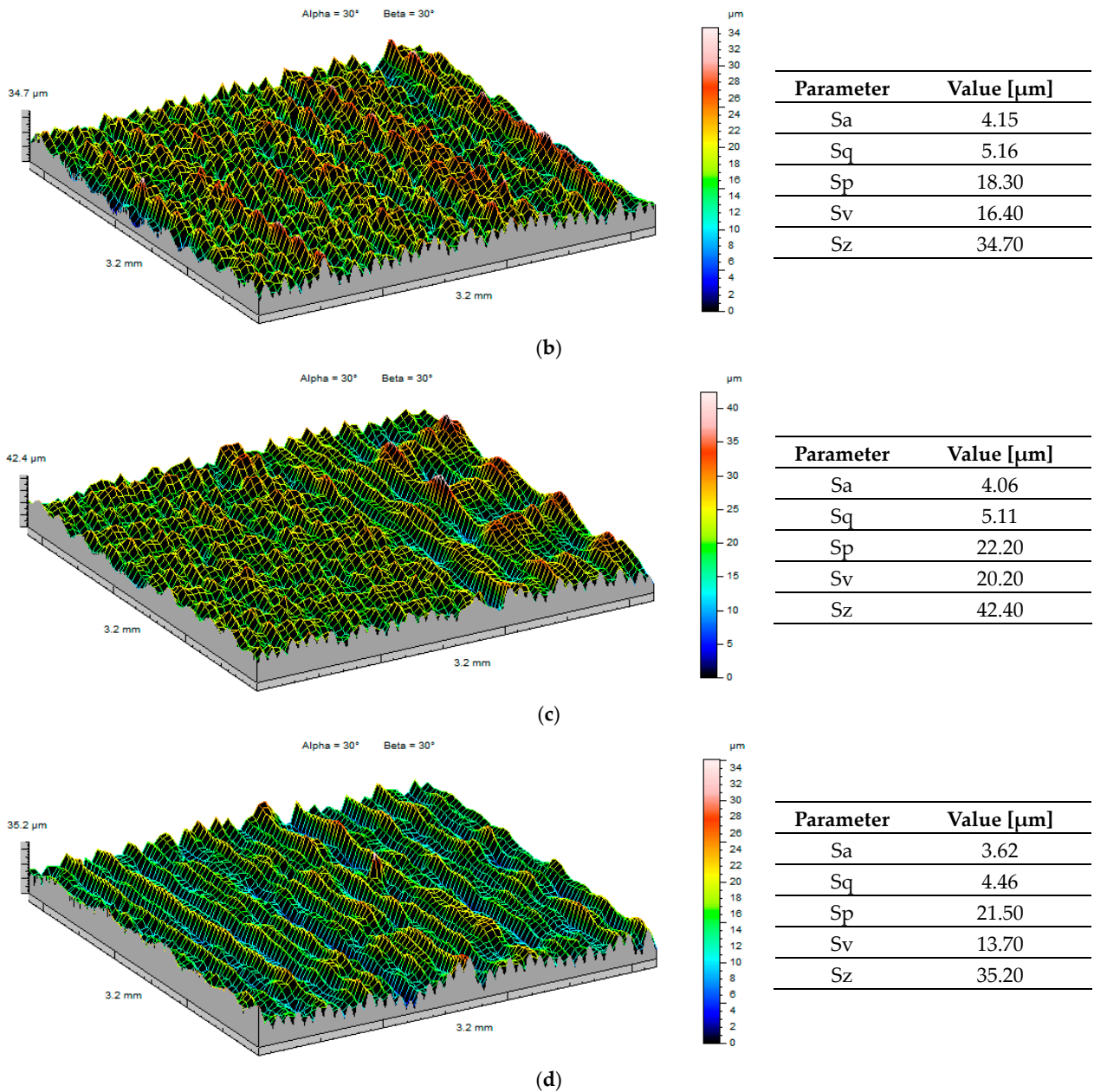


Figure 11. Results obtained evaluating the surface roughness for materials: (a) ABS Plus; (b) PLA plus; (c) PETG; (d) CPE.

4. Discussion

Considering the craniofacial area, paying attention to the data flow at the stage of modeling and manufacturing the final model is crucial. At each stage, errors occur that ultimately distinguish the fabricated anatomical structure from its actual corresponding structure (Figure 12). This difference can affect the quality of carrying out the planning and, eventually, the performance of the procedure [18,19]. The literature has pointed out that the spatial and contrast resolution of DICOM data significantly impacts the accuracy of reconstruction [20,21]. If it is impossible to obtain high-quality DICOM data, a digital processing process is performed on them. Within the scope of this article, a method of interpolation and digital filtering of the data was carried out. This process allowed for the partial recovery of lost pixels at the stage of tomographic diagnosis. Thus, the process of segmentation by thresholding was significantly improved. A triangle mesh was generated using the marching cube algorithm, enabling further CAD modeling. However, preparing

implants or surgical templates requires high surface and solid modeling skills. Crucial at this stage is the proper alignment of the designed models with the geometry of the anatomical structure [26,27]. This process is time-consuming since bony structures are not symmetrical in the sagittal plane.

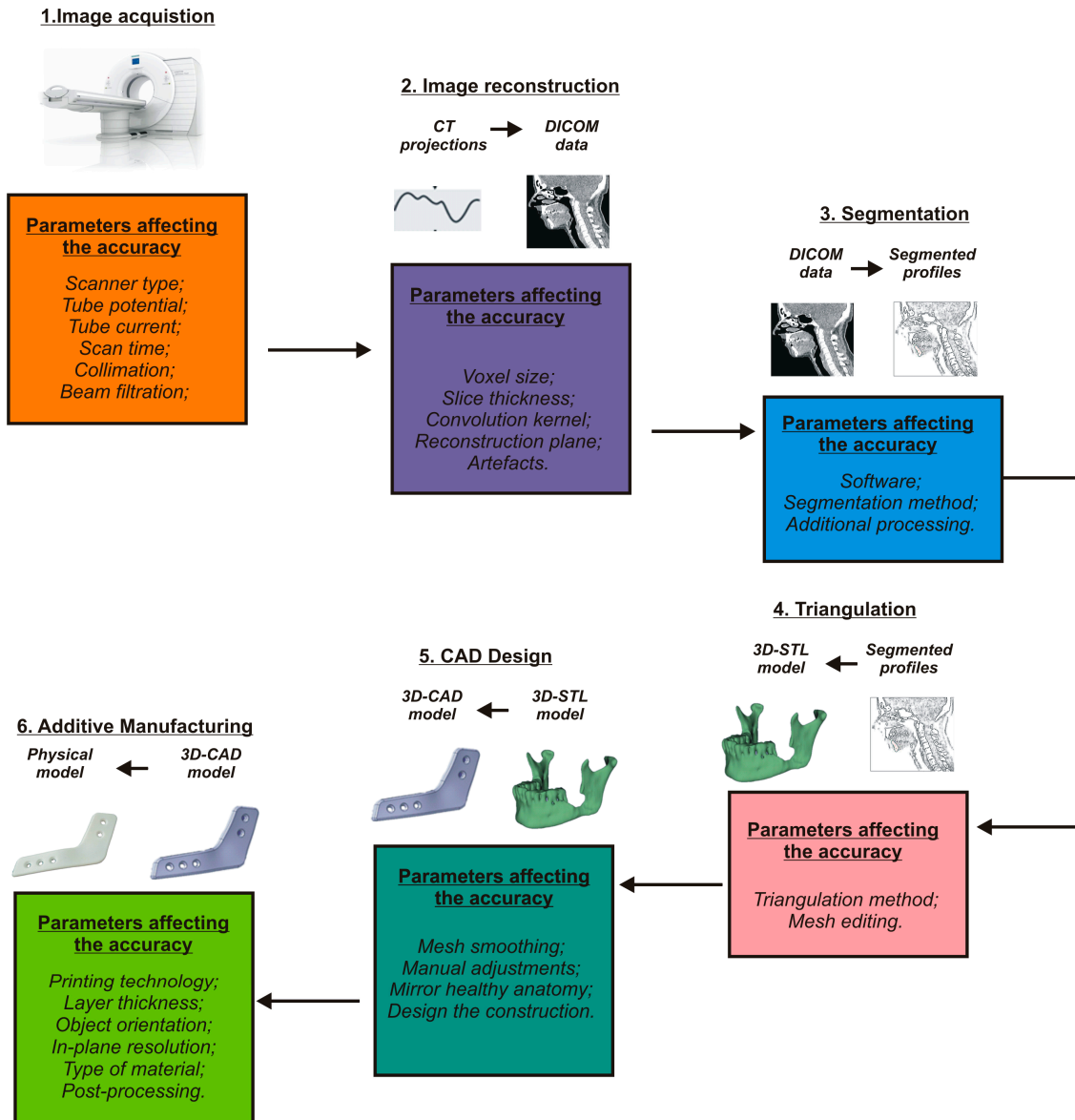


Figure 12. Factors affecting the accuracy of modeling and manufacturing of anatomical structures, surgical templates, or implants.

Various devices and methods for manufacturing models with complex shapes based on additive methods are available on the market [38,39]. Despite the availability of many additive manufacturing methods, none dominate in medical applications. This is due to several factors related to dimensional and geometry accuracy [14,35] and surface roughness [36,37]. Many factors affect the accuracy of fabricated models using additive techniques. Some of the most significant include the technology used [40,41], the thickness of the print layer [40,42], the orientation of the model in the 3D printer space [43,44], and the type of material [40,45] or finishing treatment used [37]. Recently, more and more models of anatomical structures have been made using material extrusion (MEX) techniques. The primary materials used are PLA [14,46], ABS [46], PETG [47], and polycarbonate (PC) [48]. In the case of MEX methods, the accuracy of model fabrication is usually within a tolerance

of ± 0.3 mm [49,50] and the surface roughness, traditionally expressed by the value of the Ra parameter, is highly variable and for the PLA material ranges from $0.7 \mu\text{m}$ to $12.8 \mu\text{m}$ [51], for PETG, it is from $0.91 \mu\text{m}$ to $10.64 \mu\text{m}$ [52], and for ABS, it is from $2 \mu\text{m}$ to $7 \mu\text{m}$ [53].

Nowadays, one can see the increasing use of models of anatomical structures, surgical instruments, and implants in the planning and performing of surgical procedures [9,14,38]. Also, the models made as part of the presented article support surgeons. They make the following possible:

- Better preparation of the doctor for the surgery;
- Increased precision in the performance of surgery;
- The selection of appropriate surgical instruments;
- More thorough consultation of the case with other doctors before starting the procedure;
- More detailed presentation of the scope of the surgery to the patient and a discussion of its course;
- A reduced duration of surgery (general anesthesia).

The development of models with improved modeling and manufacturing accuracy has made the precise planning of implant positions possible by avoiding blood vessels and nerves. In addition, when mapping the defect of the anterior part of the mandible and the cranial vault, the risk of damage to the adjacent bone structures is minimized.

5. Conclusions

Developing a uniform data flow in RE/CAD/RP/CAI systems is difficult. It is even more complicated when modeling anatomical structures within the craniofacial region. At each stage of the data flow, from measurement through reconstruction and CAD modeling to the execution of the physical model, geometry errors can arise. Therefore, it is essential to identify factors at these stages that affect the accuracy of the final product developed. Thus, it is possible to apply additional numerical data processing processes, increasing the accuracy of the model of the anatomical structure, the surgical template, or the implant. Through the support of CAI systems, it is possible to develop results in the form of, among other things, three-dimensional maps and statistical parameters, which enable analyses to estimate errors at the stage of manufacturing the physical model. These results provide essential information that allows quality control to be carried out on the fabricated product before it is released for immediate use.

Author Contributions: Conceptualization, P.T.; methodology, P.T., E.D., M.G. and K.W.; software, E.D., M.G. and K.W.; formal analysis, P.T.; writing—original draft preparation, P.T., E.D., M.G. and K.W.; writing—review and editing, P.T.; supervision, P.T. All authors have read and agreed to the published version of the manuscript.

Funding: This research received no external funding.

Institutional Review Board Statement: Not applicable.

Informed Consent Statement: Not applicable.

Data Availability Statement: The data will be made available by the author on request.

Conflicts of Interest: The authors declare no conflicts of interest.

References

1. Boboulos, M. CAD-CAM and Rapid Prototyping Application Evaluation. 2010. Available online: <http://sietm.com/wp-content/uploads/2015/03/cad-cam-rapid-prototyping-application-evaluation.pdf> (accessed on 14 November 2023).
2. Geng, Z.; Bidanda, B. Review of reverse engineering systems—current state of the art. *Virtual Phys. Prototyp.* **2017**, *12*, 161–172. [CrossRef]
3. Sikorska-Czupryna, S.; Mazurkow, A. The Use of Reverse Engineering to Create FEM Model of Spiroid Gears. *Adv. Manuf. Sci. Technol.* **2020**, *44*, 71–73. [CrossRef]
4. Raja, V.; Kiran, J.F. *Reverse Engineering an Industrial Perspective*; Springer: New York, NY, USA, 2010.
5. Fedorova, I.G.E.; Filimonova, T.S.; Zhuravlev, E.V.E.; Vasiliev, V.V. Estimation of the possibility of using reverse engineering in the aviation industry. *Comput. Nanotechnol.* **2019**, *6*, 68–73. [CrossRef]

6. Dúbravčík, M.; Kender, Š. Application of reverse engineering techniques in mechanics system services. *Procedia Eng.* **2012**, *48*, 96–104. [[CrossRef](#)]
7. Acher, M.; Cleve, A.; Collet, P.; Merle, P.; Duchien, L.; Lahire, P. Reverse engineering architectural feature models. In *Software Architecture: 5th European Conference, ECSA 2011, Essen, Germany, 13–16 September 2011*; Proceedings 5; Springer: Berlin/Heidelberg, Germany, 2011; pp. 220–235. [[CrossRef](#)]
8. Turek, P. Automating the process of designing and manufacturing polymeric models of anatomical structures of mandible with Industry 4.0 convention. *Polimery* **2019**, *64*, 522–529. [[CrossRef](#)]
9. Salmi, M. Additive Manufacturing Processes in Medical Applications. *Materials* **2021**, *14*, 191. [[CrossRef](#)] [[PubMed](#)]
10. Llopis-Grimalt, M.A.; Arbós, A.; Gil-Mir, M.; Mosur, A.; Kulkarni, P.; Salito, A.; Monjo, M. Multifunctional Properties of Quercitrin-Coated Porous Ti-6Al-4V Implants for Orthopaedic Applications Assessed In Vitro. *J. Clin. Med.* **2020**, *9*, 855. [[CrossRef](#)] [[PubMed](#)]
11. Abudayyeh, I.; Gordon, B.; Ansari, M.M.; Jutzy, K.; Stoletniy, L.; Hilliard, A. A practical guide to cardiovascular 3D printing in clinical practice: Overview and examples. *J. Interv. Cardiol.* **2018**, *31*, 375–383. [[CrossRef](#)]
12. Kim, J.W.; Lee, Y.; Seo, J.; Park, J.H.; Seo, Y.M.; Kim, S.S.; Shon, H.C. Clinical experience with three-dimensional printing techniques in orthopedic trauma. *J. Orthop. Sci.* **2018**, *23*, 383–388. [[CrossRef](#)]
13. Oren, D.; Dror, A.A.; Bramnik, T.; Sela, E.; Granot, I.; Srouji, S. The power of three-dimensional printing technology in functional restoration of rare maxillomandibular deformity due to genetic disorder: A case report. *J. Med. Case Rep.* **2021**, *15*, 197. [[CrossRef](#)]
14. Turek, P.; Pakla, P.; Budzik, G.; Lewandowski, B.; Przeszłowski, Ł.; Dziubek, T.; Frańczak, J. Procedure increasing the accuracy of modelling and the manufacturing of surgical templates with the use of 3D printing techniques, applied in planning the procedures of reconstruction of the mandible. *J. Clin. Med.* **2021**, *10*, 5525. [[CrossRef](#)] [[PubMed](#)]
15. Schweiger, J.; Edelhoff, D.; Güth, J.-F. 3D Printing in Digital Prosthetic Dentistry: An Overview of Recent Developments in Additive Manufacturing. *J. Clin. Med.* **2021**, *10*, 2010. [[CrossRef](#)] [[PubMed](#)]
16. Memon, A.R.; Li, D.; Hu, J.; Wang, E.; Zhang, D.; Chen, X. The development of computer-aided patient-specific template design software for 3D printing in cranio-maxillofacial surgery. *Int. J. Med. Robot. Comput. Assist. Surg.* **2021**, *17*, e2243. [[CrossRef](#)] [[PubMed](#)]
17. Ghai, S.; Sharma, Y.; Jain, N.; Satpathy, M.; Pillai, A.K. Use of 3-D printing technologies in craniomaxillofacial surgery: A review. *Oral Maxillofac. Surg.* **2018**, *22*, 249–259. [[CrossRef](#)] [[PubMed](#)]
18. Li, J.; Pepe, A.; Gsaxner, C.; Campe, G.V.; Egger, J. A baseline approach for AutoImplant: The MICCAI 2020 cranial implant design challenge. In *Workshop on Clinical Image-Based Procedures*; Springer International Publishing: Cham, Switzerland, 2020; pp. 75–84. [[CrossRef](#)]
19. Van de Velde, T.; Collaert, B.; Sennerby, L.; De Bruyn, H. Effect of implant design on preservation of marginal bone in the mandible. *Clin. Implant. Dent. Relat. Res.* **2010**, *12*, 134–141. [[CrossRef](#)] [[PubMed](#)]
20. Romans, L. *Computed Tomography for Technologists: A Comprehensive Text*; Wolters Kluwer: Baltimore, MD, USA, 2011.
21. Alsleem, H.; Davidson, R. Factors affecting contrast-detail performance in computed tomography: A review. *J. Med. Imaging Radiat. Sci.* **2013**, *44*, 62–70. [[CrossRef](#)] [[PubMed](#)]
22. Turek, P.; Filip, D.; Przeszłowski, Ł.; Łazorko, A.; Budzik, G.; Snela, S.; Paszkiewicz, A. Manufacturing Polymer Model of Anatomical Structures with Increased Accuracy Using CAX and AM Systems for Planning Orthopedic Procedures. *Polymers* **2022**, *14*, 2236. [[CrossRef](#)] [[PubMed](#)]
23. Turek, P.; Budzik, G. Development of a procedure for increasing the accuracy of the reconstruction and triangulation process of the cranial vault geometry for additive manufacturing. *Facta Univ. Ser. Mech. Eng.* **2022**. Available online: <http://casopisi.junis.ni.ac.rs/index.php/FUMechEng/article/view/7431> (accessed on 14 November 2023).
24. van Eijnatten, M.; Koivisto, J.; Karhu, K.; Forouzanfar, T.; Wolff, J. The impact of manual threshold selection in medical additive manufacturing. *Int. J. Comput. Assist. Radiol. Surg.* **2017**, *12*, 607–615. [[CrossRef](#)]
25. Huotilainen, E.; Jaanimets, R.; Valášek, J.; Marcián, P.; Salmi, M.; Tuomi, J.; Wolff, J. Inaccuracies in additive manufactured medical skull models caused by the DICOM to STL conversion process. *J. CranioMaxillofacial Surg.* **2014**, *42*, e259–e265. [[CrossRef](#)]
26. Turek, P.; Jońca, K.; Winiarska, M. Evaluation of the accuracy of the resection template and restorations of the bone structures in the mandible area manufactured using the additive technique. *Rep. Mech. Eng.* **2023**, *4*, 39–46. [[CrossRef](#)]
27. Turek, P.; Jakubiec, J. Geometrical precision and surface topography of mSLA-produced surgical guides for the knee joint. *J. Eng. Manag. Syst. Eng.* **2023**, *2*, 150–157. [[CrossRef](#)]
28. Turek, P. Evaluation of the auto surfacing methods to create a surface body of the mandible model. *Rep. Mech. Eng.* **2022**, *3*, 46–54. [[CrossRef](#)]
29. Stojkovic, M.; Veselinovic, M.; Vitkovic, N.; Marinkovic, D.; Trajanovic, M.; Arsic, S.; Mitkovic, M. Reverse modelling of human long bones using T-splines-case of tibia. *Teh. Vjesn.* **2018**, *25*, 1753–1760. [[CrossRef](#)]
30. Vitkovic, N.; Stojkovic, M.; Mitkovic, M. Designing of patient-specific implant by using subdivision surface shaped on parametrized cloud of points. *Teh. Vjesn.* **2021**, *28*, 801–809. [[CrossRef](#)]
31. Safira, L.C.; Bastos, L.C.; Estev, V.; de Azevedo, R.A.; Francischone, C.E.; Sarmiento, V.A. Accuracy of rapid prototyping biomodels plotted by three dimensional printing technique: Ex vivo study. *Adv. Comput. Tomogr.* **2013**, *2*, 41–45. [[CrossRef](#)]
32. Santolaria, J.; Jiménez, R.; Rada, M.; Loscos, F. Error compensation method for improving the accuracy of biomodels obtained from CBCT data. *Med. Eng. Phys.* **2014**, *36*, 397–404. [[CrossRef](#)] [[PubMed](#)]

33. Szymor, P.; Kozakiewicz, M.; Olszewski, R. Accuracy of open-source software segmentation and paper-based printed three-dimensional models. *J. CranioMaxillofacial Surg.* **2016**, *44*, 202–209. [[CrossRef](#)] [[PubMed](#)]
34. Brajlilh, T.; Tasic, T.; Valentan, B.; Hadžistević, M.; Pogacar, V.; Drstvenšek, I.; Balic, J.; Acko, B. Possibilities of Using Three-Dimensional Optical Scanning in Complex Geometrical Inspection. *Stroj. Vestn. J. Mech. Eng.* **2011**, *57*, 826–833. [[CrossRef](#)]
35. Budzik, G.; Turek, P.; Dziubek, T.; Gdula, M. Elaboration of the measuring procedure facilitating precision assessment of the geometry of mandible anatomical model manufactured using additive methods. *Meas. Control.* **2019**, *53*, 181–191. [[CrossRef](#)]
36. Bazan, A.; Turek, P.; Przeszlowski, Ł. Comparison of the contact and focus variation measurement methods in the process of surface topography evaluation of additively manufactured models with different geometry complexity. *Surf. Topogr. Metrol. Prop.* **2022**, *10*, 035021. [[CrossRef](#)]
37. Bazan, A.; Turek, P.; Zakrečki, A. Influence of Antibacterial Coating and Mechanical and Chemical Treatment on the Surface Properties of PA12 Parts Manufactured with SLS and MJF Techniques in the Context of Medical Applications. *Materials* **2023**, *16*, 2405. [[CrossRef](#)]
38. da Silva Júnior, E.B.; de Aragão, A.H.; de Paula Loureiro, M.; Lobo, C.S.; Oliveti, A.F.; de Oliveira, R.M.; Ramina, R. Cranioplasty with three-dimensional customised mould for polymethylmethacrylate implant: A series of 16 consecutive patients with cost-effectiveness consideration. *3D Print. Med.* **2021**, *7*, 4. [[CrossRef](#)]
39. Csámer, L.; Csernátóny, Z.; Novák, L.; Kővári, V.Z.; Kovács, Á.É.; Soósné Horváth, H.; Manó, S. Custom-made 3D printing-based cranioplasty using a silicone mould and PMMA. *Sci. Rep.* **2023**, *13*, 11985. [[CrossRef](#)]
40. Gibson, I.; Rosen, D.W.; Stucker, B. *Additive Manufacturing Technologies*; Springer: Cham, Switzerland, 2021.
41. Javaid, M.; Haleem, A. Additive manufacturing applications in medical cases: A literature based review. *Alex. J. Med.* **2018**, *54*, 411–422. [[CrossRef](#)]
42. Zhang, Z.C.; Li, P.L.; Chu, F.T.; Shen, G. Influence of the three-dimensional printing technique and printing layer thickness on model accuracy. *J. Orofac. Orthop. Fortschritte Kieferorthopadie* **2019**, *80*, 194–204. [[CrossRef](#)]
43. Abdelrhman, A.M.; Gan, W.W.; Kurniawan, D. Effect of part orientation on dimensional accuracy, part strength, and surface quality of three dimensional printed part. *IOP Conf. Ser. Mater. Sci. Eng.* **2019**, *694*, 012048. [[CrossRef](#)]
44. Arnold, C.; Monsees, D.; Hey, J.; Schweyen, R. Surface quality of 3D-printed models as a function of various printing parameters. *Materials* **2019**, *12*, 1970. [[CrossRef](#)] [[PubMed](#)]
45. Hernandez, D.D. Factors affecting dimensional precision of consumer 3D printing. *Int. J. Aviat. Aeronaut. Aerosp.* **2015**, *2*, 2. [[CrossRef](#)]
46. Yang, L.; Grottkau, B.; He, Z.; Ye, C. Three dimensional printing technology and materials for treatment of elbow fractures. *Int. Orthop.* **2017**, *41*, 2381–2387. [[CrossRef](#)]
47. Alssabbagh, M.; Abdulmanap, M.; Zainon, R. Evaluation of 3D printing materials for fabrication of a novel multi-functional 3D thyroid phantom for medical dosimetry and image quality. *Radiat. Phys. Chem.* **2017**, *135*, 106–112. [[CrossRef](#)]
48. Favier, V.; Zemiti, N.; Caravaca Mora, O.; Subsol, G.; Captier, G.; Lebrun, R.; Gilles, B. Geometric and mechanical evaluation of 3D-printing materials for skull base anatomical education and endoscopic surgery simulation—A first step to create reliable customized simulators. *PLoS ONE* **2017**, *12*, e0189486. [[CrossRef](#)] [[PubMed](#)]
49. Herath, B.; Suresh, S.; Downing, D.; Cometta, S.; Tino, R.; Castro, N.J.; Hutmacher, D.W. Mechanical and geometrical study of 3D printed Voronoi scaffold design for large bone defects. *Mater. Des.* **2021**, *212*, 110224. [[CrossRef](#)]
50. Zakani, S.; Chapman, C.; Saule, A.; Cooper, A.; Mulpuri, K.; Wilson, D.R. Computer-assisted subcapital correction osteotomy in slipped capital femoral epiphysis using individualized drill templates. *3D Print. Med.* **2021**, *7*, 18. [[CrossRef](#)] [[PubMed](#)]
51. Mendricky, R.; Fris, D. Analysis of the accuracy and the surface roughness of fdm/fff technology and optimisation of process parameters. *Teh. Vjesn.* **2020**, *27*, 1166–1173. [[CrossRef](#)]
52. Barrios, J.M.; Romero, P.E. Improvement of surface roughness and hydrophobicity in PETG parts manufactured via fused deposition modeling (FDM): An application in 3D printed self-cleaning parts. *Materials* **2019**, *12*, 2499. [[CrossRef](#)]
53. De León, A.S.; Domínguez-Calvo, A.; Molina, S.I. Materials with enhanced adhesive properties based on acrylonitrile-butadiene-styrene (ABS)/thermoplastic polyurethane (TPU) blends for fused filament fabrication (FFF). *Mater. Des.* **2019**, *182*, 108044. [[CrossRef](#)]

Disclaimer/Publisher’s Note: The statements, opinions and data contained in all publications are solely those of the individual author(s) and contributor(s) and not of MDPI and/or the editor(s). MDPI and/or the editor(s) disclaim responsibility for any injury to people or property resulting from any ideas, methods, instructions or products referred to in the content.